Evaluating Stress Distribution and Wear Patterns during Jogging Gait Cycle of a Hip Implant: A Finite Element Analysis

Kalayarasan M (PhD)[1], Dhanabal P (PhD)[1], Rahul V (B.E)[1], Kavin D (B.E)[1], Jonathan Reginald (M.E)[1], Nishant Nikam (M.Tech)[2], Chethan K N (PhD)[2]*

[1]Department of Mechanical Engineering, PSG College of Technology, Coimbatore, Tamil Nadu, India
[2]Manipal Institute of Technology, Manipal Academy of Higher Education, Manipal, Karnataka, India

ABSTRACT

Background: Total Hip Arthroplasty (THA) is a common surgical procedure used to restore joint function. However, maintaining implant longevity and reducing wear remain major challenges, particularly under dynamic, high-impact activities.

Objective: This study aimed to evaluate the mechanical performance of a newly designed hip implant to enhance durability during activities.

Material and Methods: In this analytical study, a new hip implant configuration was analysed using finite element methods to assess stress distribution, wear, and fatigue life. Radial clearance effects were examined, and wear estimation was performed using Archard's model. The fatigue performance of Ti-6Al-4V alloy and the liner behaviour of Ultra-High-Molecular-Weight Polyethylene (UHMWPE) were compared to conventional materials.

Results: Optimizing the design, a 0.2-millimetre radial clearance reduced contact pressure and improved implant durability. The material selection also contributed significantly: Ti-6Al-4V provided superior fatigue safety margins for high-impact loads, while UHMWPE liners significantly reduced wear rates. Overall, the CoCr-UHMWPE-Ti-6Al-4V combination achieved enhanced mechanical stability, wear resistance, and fatigue life.

Conclusion: The optimized implant configuration demonstrates promising mechanical performance for active THA patients. Further experimental and clinical validation is necessary to confirm long-term safety and durability before clinical implementation.

Keywords

Arthroplasty; Finite Element Analysis; Femoral Head Prosthesis; Radial Clearance; Hip Prosthesis; Jogging

Introduction

The hip joint is a crucial ball-and-socket joint that links the femoral head to the acetabulum of the pelvis, offering stability while allowing movement and bearing body weight [1]. The hip bone consists of the ilium, ischium, pubis, and acetabular bones, forming the acetabulum, where the femoral head articulates [2], where joint is essential for bearing the upper body's weight during activities, such as sitting, standing, stair ascending-descending, and walking, and

*Corresponding author:
Chethan K N
Manipal Institute of Technology, Manipal Academy of Higher Education, Manipal, Karnataka, India
E-mail: chethan.kn@manipal.edu

Received: 10 July 2025
Accepted: 3 December 2025

transferring weight to the lower extremities for locomotion [3-5]. Biomechanics play a vital role in understanding the forces, moments, and movements within the hip joint, to develop devices for joint replacement and fracture fixation [6]. Additionally, advancements in hip joint replacement technology, such as porous tantalum products, have enhanced biocompatibility and synovial fluid retention, and have also improved the effectiveness of hip joint implants [7]. Some solutions to hip joint problems have been proposed, including a motion assist device designed to provide an assist force to the hip joint without restricting natural movement [8], an artificial hip joint with features to prevent bone dislocation, a hip joint exercise device for targeted hip joint flexibility exercises [9], and ongoing research on optimal material combinations for hip joint prostheses [10]. Additionally, an artificial hip joint design was developed to improve bone-retaining and initial fixation capabilities [11]. These solutions address different aspects of hip joint issues, from mobility assistance and exercise to material science advancements in prosthetic hip joints, showcasing a multi-dimensional approach for tackling hip joint problems.

Total Hip Arthroplasty (THA), as an effective surgical procedure for hip joint issues, is dubbed "the operation of the century" due to the enhancement of patients' quality of life [12]. THA has recently evolved, with advancements in techniques, implants, and safety measures contributing to its success and increased longevity, even in younger and more active patients [13]. However, complications, such as metallosis, can arise post-THA, particularly in metal-on-metal implants, leading to tissue damage, pseudotumor formation, and the need for revision surgery to prevent further bone loss and necrosis [14]. Surgeons must consider various factors, such as implant stability, spinopelvic relationship, and abnormal pathologies, to ensure successful outcomes and reduce postoperative risks in THA [15]. Polymers, metal alloys, and ceramics are the most widely used biomaterials for THA, which substitute damaged joint surfaces with synthetic material [16].

The biomaterials play a key role in THA success [16], affecting mechanical properties, survivability, and sterilization methods [17]. The average lifespan of artificial hip joints is approximately 15 years, according to research, necessitating continued advancements aimed at maximizing longevity and reducing complications [18]. Studies have also highlighted the importance of selecting the appropriate bearing surfaces in THA procedures to reduce the risk of revision, with materials, such as highly Cross-linked Polyethylene (XLPE), delta ceramic, and oxidized zirconium, showing lower revision rates than cobalt chrome and stainless steel [19]. The design of THA involves various aspects, such as stem design, biomechanical considerations, material selection, and patient outcomes. Stem design in THA can impact knee biomechanics, with short stems associated with better outcomes in terms of knee valgus deformity [20].

The biomechanical properties of the femoral component play a crucial role in stress shielding and physiological strain transfer during THA, highlighting the importance of stem stiffness and design [21]. Additionally, the development of femoral stem prostheses has evolved, with materials, such as Ti-6Al-4V, Cobalt Chromium, and stainless steel to improve performance and reduce complications [22]. Given the identical survival rates and failure hazard ratios across single- and dual-taper stem designs in THA, the evidence further highlights the crucial role of stem-focused goals in determining patient outcomes [23]. Digital solutions that improve open adherence and communication across the THA experience may be developed by including patient demands through a co-design approach [24]. End-stage arthritic hip problems can be successfully resolved by THA, which improves performance and relieves discomfort [25].

Despite the success of THA, challenges like limb length discrepancy persist, requiring reliable techniques to minimize postoperative issues. As THA approaches its fourth decade, research continues to focus on addressing complications and improving outcomes in patients with coxarthrosis [26].

Design solutions for THA involve various aspects, such as the use of Patient-Specific Instruments (PSIs) to enhance surgical accuracy [27], the consideration of different implant designs for optimal outcomes and longevity, and the development of patient-specific acetabular cages to address severe defects and improve fixation [28]. The implants are typically composed of a femoral component made of cobalt-chromium or titanium alloys and an acetabular component with a metallic shell and Ultra-High-Molecular-Weight Polyethylene (UHMWPE) liner [29].

The success of THA relies on a combined strategy of optimized implant design and advanced post-operative care. Implant design focuses on achieving primary stable fixation through specific shapes, proportions, and surface structures, thereby allowing for bone ingrowth and successful long-term outcomes [30]. Furthermore, material solutions and coatings are essential for improving the functionality and durability of the prostheses. The overall efficacy is further enhanced by integrating telemedicine technologies, which improve postoperative care by enabling remote monitoring and regular contact with specialists, potentially reducing complications and treatment costs [31]. The overall efficacy and success of THA are enhanced by these combined strategies. Material solutions and coatings are essential for improving the functionality and durability of THA hip prostheses.

Some materials, such as metals, ceramics, and polymers, have been developed for hip implants with recent advancements in bioceramic coatings to improve biocompatibility, wear resistance, and toughness [32]. Coatings like Titanium Nitride (TiN) and diamond-like carbon improve osseointegration and prevent complications, such as osteolysis, by creating passivation layers and lowering the inflammation caused by wear particles [33]. Moreover, the development of local implant coatings and advancements in bearing surface technologies have been introduced to address issues such as periprosthetic joint infection, a significant cause of THA failure, emphasizing the importance of selecting suitable materials and coatings to maximize implant success rates [34]. Factors, such as patient demographics (age, Body Mass Index (BMI), gender), bone mineral density, preoperative psychological status (depression, anxiety), surgical techniques (cemented vs. uncemented), and postoperative complications play crucial roles in determining the success of THA procedures [35]. Studies have highlighted the importance of considering individual patient characteristics, including BMI, comorbidities, surgical approach, and age, in predicting postoperative outcomes in patients undergoing THA. Research correlating Bone Mineral Density (BMD) levels with postoperative efficacy, and the impact of preoperative psychological factors on pain and functional outcomes after THA, highlights the multifactorial effects for surgical success.

Surgeons should consider these factors to optimize patient counselling and treatment strategies to improve THA outcomes. To enhance patient comprehension and health literacy, it is essential to improve the readability of patient education materials related to THA [36]. The future scope of THA treatment involves advancements in bearing surfaces, surgical techniques, and technology. Ideal THA-bearing surfaces should prioritize wear resistance, durability, bio-inertness, cost-effectiveness, and ease of implantation. Additionally, improvements in THA design, such as utilizing large femoral heads, dual-mobility cups, and different bearing surface combinations, can reduce wear and impingement [37]. Highly accurate acetabular placement is made possible by cutting-edge robotic technology, and

THA results are improved by patient-specific instrumentation and dual-mobility bearings [38]. National THA registers play a crucial role in documenting quality, providing benchmarks, and facilitating research and post-market surveillance to ensure best practices and report implant outliers [39].

Previous studies have provided valuable insights into hip implant performance under static or simplified loading conditions; however, it is needed to evaluate implant behavior under dynamic, high-impact activities such as jogging, which are increasingly relevant for active patients [5,40]. Earlier works primarily focused on static load analyses or conventional gait cycles with limited emphasis on impact activities. Material properties and sensitivity analyses were explored [1,41], but the influence of higher forces or optimized design parameters for such scenarios was not specifically addressed.

To develop long-lasting hip implants for active patients, this study models the jogging gait cycle to simulate complex dynamic loads, a distinguishing feature. This research aimed to assess how radial clearance affects stress distribution, wear rates, and fatigue life. Furthermore, it compares various material combinations, focusing on Ti-6Al-4V alloy with UHMWPE liners, to identify configurations that offer superior durability and wear resistance. The present research work supports the Sustainable Development Goals (SDGs) 3, and 9, which ensuring good health and well-being, and fostering industry, innovation and infrastructure, respectively.

Material and Methods

The New Hip Implant Design

This analytical study demonstrates that variations in implant design parameters, specifically neck diameter, stem cross-section, and stem length, are critical determinants of the implant's overall performance. The hip implant design utilized in this study Figure 1 carefully considered these factors. The specific dimensions, including femoral head diameter, neck dimensions, and stem length, are detailed in Table 1. These standardized measurements form the foundation for the Finite Element Analysis (FEA), ensuring the simulated implant geometry reflects realistic, clinically relevant configurations [41]. This advanced design was meticulously crafted using the commercial Computer-Aided Design (CAD) software, SolidWorks 2021. Radial clearances between the stem and femoral head junction, set at 0 mm, 0.1 mm, 0.2 mm, and 0.3 mm, are considered to provide a flawless fit. Meanwhile, there was no space separating the liner-acetabular and femoral head-liner interfaces, ensuring a snug and stable connection, like the perfect fit of a well-engineered running shoe.

Materials

Materials, such as biomaterials that ensure a smooth, pain-free jog, are crucial for THA. The most widely used biocompatible materials include titanium alloys, Cobalt-Chromium

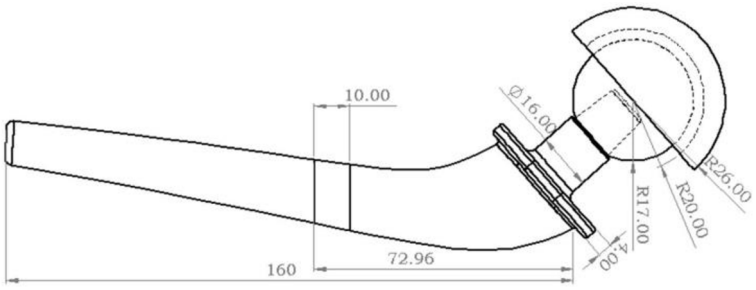

Figure 1: Geometric representation of the customized hip implant.

Table 1: Design parameters for the hip implant study

Design Parameters	Dimension (mm)
Diameter of the femoral head	34
Length of neck	14
Diameter of the neck (Top)	12
Diameter of the neck (Base)	14
Stem length	160

(CoCr) alloys, stainless steel, alumina, and UHMWPE [42]. Material Combinations (MC) listed in Table 2, outlining different configurations of acetabular cup, liner, femoral head, and stem materials for the hip implant design [40]. These materials were selected for their well-documented ability to withstand the dynamic stresses of activities such as jogging.

Table 3 presents a comprehensive summary of the material properties, assumed to be homogeneous and exhibiting linear elastic behaviour to ensure consistent mechanical performance under each loading cycle. Parameters such as Young's modulus, density, Poisson's ratio, and ultimate tensile strength serve as essential inputs for the FEA, enabling the simulations to replicate realistic mechanical responses [43].

Gait cycle

Jogging has been recognized as a beneficial activity for the improvement of cardiovascular health and overall fitness, differentiated from running by its lower intensity, reduced energy expenditure, and less strain on the heart, lungs, and muscles. Both jogging and running were classified as aerobic exercises that utilized oxygen, blood sugar, or body fat as energy sources. The phases of movement and load distribution during the jogging gait cycle were illustrated in Figure 2. In this analysis, only the force data corresponding to one gait cycle of jogging were considered Figure 3. The significantly large moment data associated with jogging would have required a separate, specialized computational algorithm for an effective solution, which was beyond the scope of this study.

Table 2: Material combinations employed for the hip implant design, showcasing the various configurations.

Material Combinations	Stem	Femoral Head	Liner	Acetabular Cup
MC1	CoCr Alloy	CoCr Alloy	UHWMPE	CoCr Alloy
MC2	CoCr Alloy		CoCr Alloy	
MC3	Ti-6Al-4V Alloy		UHWMPE	
MC4	Ti-6Al-4V Alloy		CoCr Alloy	

UHMWPE: Ultra-High-Molecular-Weight Polyethylene, MC: Material Combinations, CoCr: Cobalt-Chromium

Table 3: Overview of the mechanical properties of materials utilized in the hip implant designs.

Sl. No.	Materials	Young's modulus (GPa)	Density (gm/cm^3)	Poisson's ratio	Ultimate tensile strength (MPa)
1.	Ti-6Al-4V alloy	120	4.5	0.33	930
2.	CoCr alloy	200	8.5	0.3	1503
3.	UHMWPE	0.96	0.94	0.31	48

CoCr: Cobalt-Chromium, UHMWPE: Ultra-High-Molecular-Weight Polyethylene

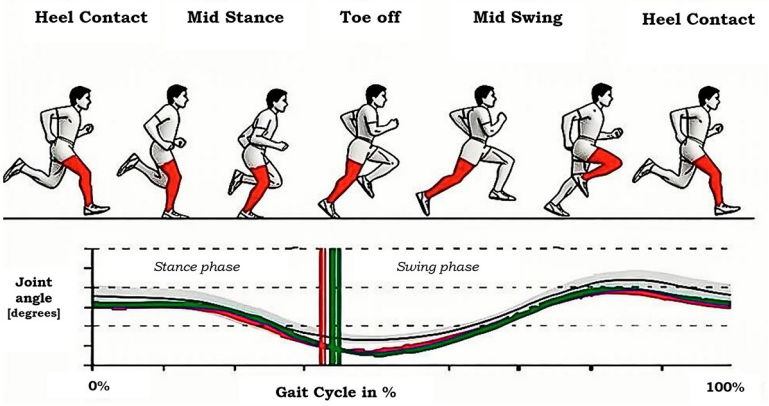

Figure 2: Jogging gait cycle, representing the phases of movement and load distribution. Reproduced with permission from Tirosh O. 2016 [44].

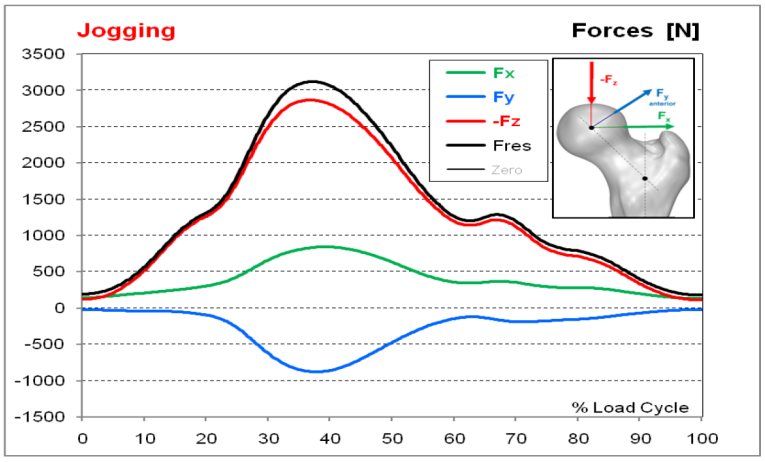

Figure 3: Loads during one gait cycle of jogging. Reproduced with permission from Bergmann et al. 2016 [45].

Wear estimation

The sliding wear growth on articulating surfaces was predicted using the Archard wear model, as follows (Equation 1):

$$W_v = K_W F S \quad (1)$$

where, S, F, K_w, and W_V refer to the sliding distance between the contacting surfaces, applied contact load, wear coefficient discovered during the study, and volumetric wear of the bearing surface, respectively. Equation (2) may be used to determine the linear wear W_L on the surface by dividing both sides by an area (A), where P stands for contact stress in the manner described below:

$$W_L = K_W P S \quad (2)$$

The volumetric and linear wear rates across the trunnion and head interfaces were evaluated. The units of measurement for the volumetric and linear wear rates were mm^3/year and mm/year, respectively. The interacting surface area between the head and trunnion measures 1025.09 mm^2 with a push fit and 452.16 mm^2 with a radial clearance fit. The top surface diameter of the trunnion was 12 mm with a contact length of 14 mm with the head. Equations (3) and (4) were used to determine the linear and volumetric wear rates for one million cycles.

$$W_L = K_w P S \times 10^6 \, (mm/10^6 \text{ cycles}) \quad (3)$$

$$W_V = K_L A \times 10^6 \, (mm/10^6 \text{ cycles}) \quad (4)$$

Finite element model

The analysis was carried out using ANSYS Workbench R19.2. As shown in Figure 4 (a), an impact force of 4000 N was applied in the first section, where the stem was fully fastened [37]. This arrangement aimed to replicate the procedure of a surgeon joining the femoral head prosthesis and stem by applying force to the femoral head using a mallet during the surgical procedure [46]. Following ASTM F2996-13, boundary conditions for the second segment were established by defining its position on the stem. Specifically, a reference line was drawn at 80 mm and 90 mm from the tip of the stem [47]. The fixed stem portion was located beneath the 90 mm reference line.

Throughout this study, frictional interactions were employed at several interfaces. The ASTM F2996-13 loading and boundary requirements are depicted in Figure 4 (b), and the discretized mesh model of the implant is displayed in Figure 4 (c). A mesh convergence study was conducted to determine the ideal mesh size [48]. In one-millimetre increment, the mesh sizes ranged from 5 mm to 1 mm. When von Mises stresses were assessed for mesh size conclusions, it was determined that stress variations were negligible for mesh sizes under two-millimetre. As a result, a 2-mm mesh size was selected for the analysis. Hexahedral components were utilized in this study, and the final mesh contained 33,081 elements and 114,847 nodes.

Two Kistler plates measuring the ground response forces were used to record the force and moment that the implant encountered [49]. Table 4 presents experimentally derived Coefficients of Friction (COF) and wear coefficients (K_w) for key material pairings in hip implants, including CoCr–CoCr, CoCr–Ti-6Al-4V, and CoCr–UHMWPE. These tribological parameters are critical inputs for the finite element simulations in the study, as they directly influence wear predictions, contact stress

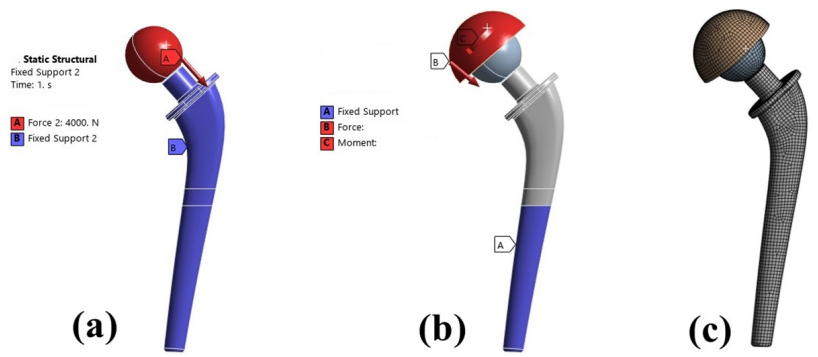

Figure 4: **a**) Impact load analysis on the hip implant head, **b**) illustrating the Loading and Boundary conditions, **c**) Discretized model representation provides insights into stress distribution under physiological conditions

Table 4: Coefficient of Friction (COF) and coefficient of wear (Kw) for materials investigated

Combination of materials	Coefficient of Friction	Wear Coefficient (Kw) (mm^3/Nm)
CoCr-CoCr	0.2	$1.68e^{-5}$
CoCr-Ti-6Al-4V	0.24	$1.31e^{-5}$
CoCr-UHMWPE	0.15	$3.5e^{-7}$

CoCr: Cobalt-Chromium, UHMWPE: Ultra-High-Molecular-Weight Polyethylene

modelling, and comparative performance evaluations between different material combinations [50].

Fatigue analysis

Well-designed implants require an indefinite or maximum fatigue life. This study used FEA to assess the fatigue life and safety parameters of hip implants under various gait loadings and material combinations. The S-N curves for the tested materials, Ti-6Al-4V alloy and CoCr alloys, are presented in Figure 5 [51]. As shown in Equations (5) and (6), the mean stress (σ_m) and alternating stress (σ_a) are characterized by the maximum stress (σ_{max}) and minimum stress (σ_{min}) per Goodman's mean stress fatigue theory [52].

$$\sigma_m = \frac{\sigma_{max} + \sigma_{min}}{2} \quad (5)$$

$$\sigma_a = \frac{\sigma_{max} + \sigma_{min}}{2} \quad (6)$$

$$\frac{1}{Nf} = \frac{\sigma_a}{Se} + \frac{\sigma_m}{Su} \quad (7)$$

Equation (7) illustrates the application of Goodman's theory to obtain the factor of safety (N_f) according to alternating stress (σ_a), mean stress (σ_m), endurance limit (S_e), and ultimate tensile strength (Su). The S-N curve indicates that if a material remains below its stress limit, it will survive its life cycle. The fatigue life and safety factor of the assembled components were determined using the ANSYS Workbench R19.2 fatigue tool within the static structural module.

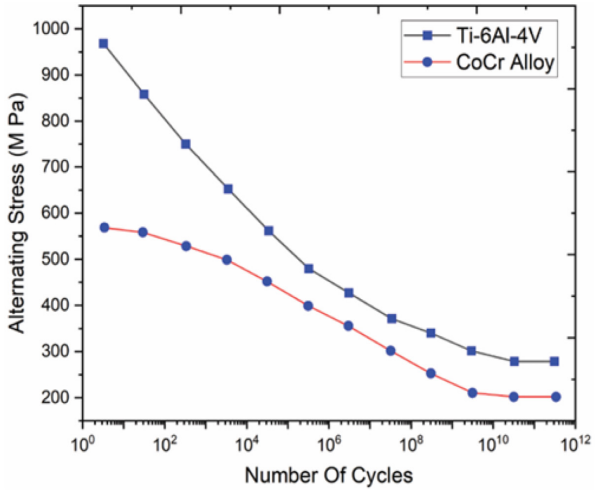

Figure 5: S-N curve for Ti-6Al-4V alloy and CoCr alloy. Permission from Reginald et al. 2023 [40].

Results

Static analysis

Static analysis evaluates the hip implant integrity under physiological loads. The total deformation assesses displacement, von Mises stress predicts material failure, and strain analyses elasticity. Excessive stress or strain can cause wear, loosening, or fracture, thereby reducing longevity. This study optimizes implant design for better load distribution, stability, and durability, ensuring reliable performance in high-impact activities, such as walking and jogging.

Total deformation

The impact analysis performed in the initial stage yielded consistent results [41], thereby validating the accuracy of the approach. The next step of the study focused on analysing the dynamic load during the jogging gait cycle, which is crucial for assessing the hip implant performance. Figure 6 (a-c) depict the total deformation, von Mises stress, and strain, respectively. This strain was within the implant components under dynamic loading conditions during the jogging gait cycle. The maximum deformation recorded was 0.0238 mm for MC1, at a radial clearance of 0.3 mm. In terms of von Mises stress, the highest value of 114.11 MPa was at a radial clearance of 0 mm.

Figure 7 demonstrates the relationship between radial clearance and total deformation, a critical factor influencing wear and durability. This analysis confirms the pivotal role radial clearance plays in optimizing hip implant performance during high-impact activities, such as jogging. Specifically, the data indicate

that deformation increases at a 0.1 mm clearance, while optimal performance is achieved at a clearance of 0.2 mm.

Dynamic analysis

Dynamic analysis is essential for evaluating the mechanical performance of well-designed prostheses, particularly in hip joint replacements, where multiple interfaces influence the overall functionality. Key junctions such as the Femoral Head - Stem (HS), Femoral Head - Liner (HL), and Liner-Acetabular (LA), experience varying contact pressures during movement. The variation in sliding distance with changes in radial clearance significantly affects wear and stability, particularly during high-impact activities, such as jogging. These dynamic interactions help to optimize prosthetic design, ensuring durability, reduced wear, and enhanced patient mobility.

1. Differences in contact pressure across various interfaces

Figure 8 (a) shows the contact pressure (MPa) exerted at the HS junction. The maximum pressure reached 45.437 MPa, concentrated near the upper contact region, while the

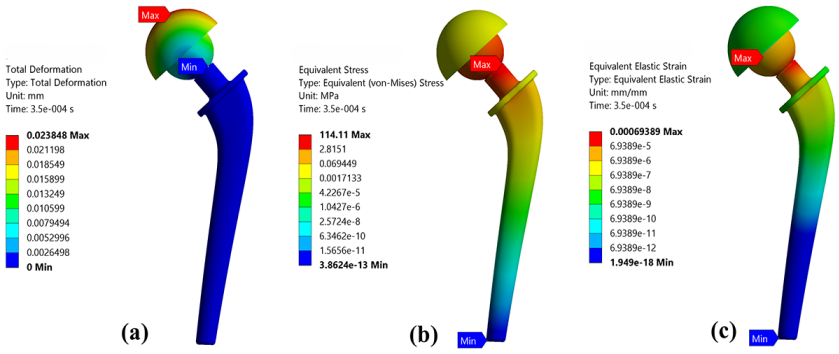

Figure 6: **a**) Total deformation, **b**) von Mises stress distribution, **c**) Equivalent elastic strain within the implant components under dynamic loading conditions during the jogging gait cycle

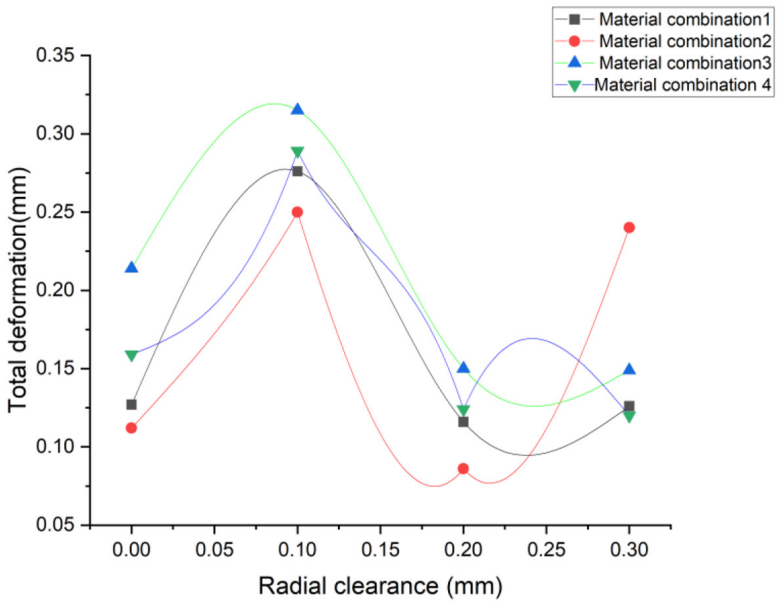

Figure 7: Graphical representation of total deformation changes with radial clearance changes

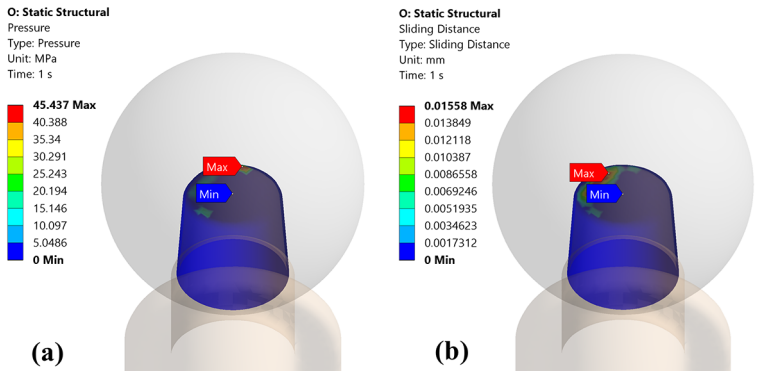

Figure 8: **a**) Illustrates the contact pressure, **b**) Sliding distance at the Femoral Head - Stem (HS) junction.

rest of the junction experienced a gradually lower pressure, down to 0 MPa. This gradient highlights the localized stress zones, which are critical for wear prediction and implant integrity. Figure 8 (b) shows the relative sliding distance (mm) at the same HS junction. The maximum sliding distance was 0.01558 mm, occurring near the upper contact area (marked in red), tapering off to 0 mm in the lower section. This spatial variation is essential for evaluating potential wear regions, particularly during dynamic activities such as jogging.

Figure 9 (a) shows the contact pressure at the HL junction. The maximum pressure reached 0.48901 MPa, located centrally, indicating the primary load-bearing zone. The pressure decreased radially outward, with minimum values near the edges, signifying reduced load transfer in the peripheral regions. Furthermore, the maximum sliding distance recorded was 0.022045 mm, appearing at the peripheral edge, while the minimum was located opposite to the high-motion zone. This distribution shows asymmetric joint articulation during jogging, which can inform wear-path predictions.

Figure 9 (b) shows the contact pressure (MPa) at the LA interface. The maximum pressure was approximately 0.37774 MPa, which was observed near the upper-central region (marked in red). The minimum pressure appears at the lower peripheral area (in blue, ~0 MPa), indicating a non-uniform load distribution across the surface, which may impact the long-term liner wear behaviour. The second subplot illustrates the sliding distance (in mm), with a maximum value of 0.015219 mm at the outer edge of the articulation zone (in red). The minimum displacement (~0 mm, blue) is situated on the opposite side. This gradient indicates a clear directional sliding pattern caused by joint kinematics during jogging.

Table 5 presents the effect of material combinations and variation on contact pressure as the radial clearance changes at the HS junction. MC1 exhibited the highest initial contact pressure (146.12 MPa) at 0 mm, but this pressure sharply decreased as the radial clearance increased, reaching nearly zero at 0.2 mm. Similarly, MC2 starts with a slightly lower pressure (114.45 MPa) at 0 mm, following the same trend and dropping to negligible levels at 0.2 mm. MC3 showed a moderate initial pressure (99.04 MPa), but decreased rapidly with increasing clearance, showing the first two combinations. In contrast, MC4 starts with the lowest pressure (89.92 MPa) at 0 mm, with a more gradual reduction.

The fluctuation of the peak contact pressure in response to changes in the radial clearance at the HL junction shows that the analysis of contact pressures across different material combinations reveals distinct trends. MC2 and

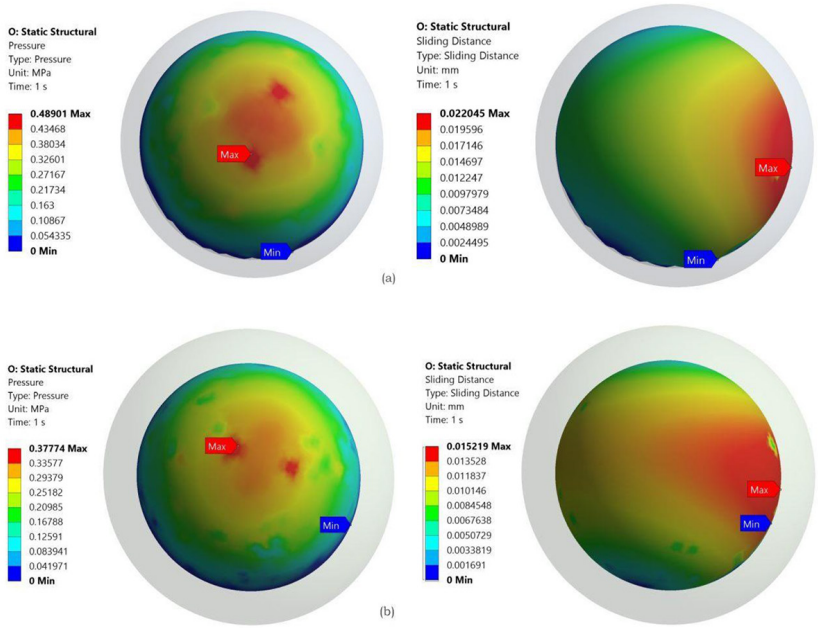

Figure 9: a) Illustrates the contact pressure and sliding distance variations at the Femoral Head - Stem (HS) junction, **b)** contact pressure and sliding distance at the Liner-Acetabular (LA) junction.

MC4 began with a high contact pressure of approximately 52 MPa at 0 mm radial clearance, and MC1 and MC3 across all clearances showed the lowest contact pressure.

Furthermore, variation in radial clearance between the liner and acetabular junction and variations in contact pressure exhibited unique characteristics. MC2 starts with a high contact pressure (18.44 MPa) at a radial clearance of 0.1 mm, MC1 and MC3 across all clearances showed the lowest contact pressure.

2. Variation of Sliding Distance with change in radial clearance

With respect to hip implants, wear and implant longevity are greatly influenced by the sliding distance between parts, such as the HS, HL, and LA. Table 6 shows that the LA junction exhibits the highest sliding distances to 0.09 mm (MC2, 0.3 mm clearance). In contrast, the HL and LA interfaces maintained consistently low sliding distances of 0.00087 mm (MC2, 0 mm clearance). Material combinations MC2 and MC4 generally demonstrate lower sliding distances, indicating better overall performance in terms of wear reduction.

MC2 and MC3 were the most effective for the HS junction, while MC1 and MC4 showed lower sliding distances across all parts.

Fatigue analysis

Fatigue analysis ensures the durability of mechanical structures, especially prostheses, by assessing the repeated loading effects. Dynamic analysis helps to understand stresses during activities, such as jogging and optimizing material selection and design. Because jogging involves continuous impact forces and varying gait dynamics, a detailed fatigue assessment helps predict potential failure points, enhance user comfort, and improve the overall functionality.

1. Fatigue characteristics of the new hip implant

A high fatigue life should be guaranteed by a well-designed prosthesis, particularly when subjected to dynamic and repeated stresses encountered during jogging. Fatigue analysis

Table 5: Variation of contact pressure between hip implant components as a function of radial clearance

Material Combinations	Radial Clearance (mm)	HS - Contact Pressure (MPa)	HL - Contact Pressure (MPa)	LA - Contact Pressure (MPa)
MC1	0	146.12	0.489	0.385
	0.1	37.49	0.504	0.436
	0.2	13.38	0.536	0.397
	0.3	45.44	0.489	0.38
MC2	0	99.04	52.71	2.78
	0.1	37.46	13.98	18.44
	0.2	13.39	16.1	16.47
	0.3	29.62	9.25	10.42
MC3	0	114.45	0.579	0.409
	0.1	34.94	0.506	0.438
	0.2	12.61	0.54	0.397
	0.3	80.02	0.489	0.422
MC4	0	89.92	52.71	2.79
	0.1	34.85	14.36	17.769
	0.2	12.63	16.12	16.47
	0.3	91.11	17.836	8.25

MC: Material Combinations, HS: Femoral Head - Stem, HL: Femoral Head - Liner, LA: Liner-Acetabular

was performed on all the models in this study, with the S-N curve shown in Figure 5, which is a key factor in determining the performance. The Goodman equation (Equation 6) was applied to evaluate the fatigue life and safety factor. The results are depicted in Figure 10 (a) for the safety factor across various radial clearances and Figure 10 (b) for the fatigue life for different material combinations.

The first subplot illustrates the Factor of Safety (FoS) across the different radial clearances. The FoS values span from a maximum of 15 (deep blue, signifying very high safety) down to a minimum of 2.1828 (green-to-red, highlighting critical regions near the stem neck). These results indicate that while most areas remain within safe limits under repetitive loading, the localized stress concentrations may warrant material optimization. The second subplot, in turn, reflects the performance of various material combinations by showing the fatigue life with respect to the number of cycles.

The maximum fatigue life reached approximately 2.271×10^{10} cycles, with the lowest values nearing 1.0×10^{8} cycles in the femoral neck region (red zone). The findings indicate that, despite the overall durability of the implant structure, localized, stress-prone regions may be vulnerable to failure under extended use, underscoring the need for material or geometric optimization.

Figure 11 illustrates the relationship between the radial clearance (mm) and the FoS for various material combinations, demonstrating optimal performance metrics at a clearance of 0.2 mm, critical for minimizing wear and maximizing implant longevity.

Table 6: Variation of sliding distances between hip implant components as a function of radial clearance

Material Combinations	Radial Clearance (mm)	HS - Sliding Distances (mm)	HL - Sliding Distances (mm)	LA - Sliding Distances (mm)
MC1	0	0.022	0.027	0.016
	0.1	0.012	0.026	0.016
	0.2	0.014	0.024	0.0146
	0.3	0.016	0.022	0.015
MC2	0	0.016	0.0045	0.00087
	0.1	0.012	0.0086	0.0061
	0.2	0.015	0.0052	0.0059
	0.3	0.016	0.01	0.09
MC3	0	0.039	0.031	0.015
	0.1	0.014	0.025	0.015
	0.2	0.015	0.023	0.0143
	0.3	0.013	0.025	0.014
MC4	0	0.02	0.0046	0.00088
	0.1	0.014	0.0077	0.0054
	0.2	0.015	0.0052	0.006
	0.3	0.01	0.0111	0.0045

MC: Material Combinations, HS: Femoral Head - Stem, HL: Femoral Head - Liner, LA: Liner-Acetabular

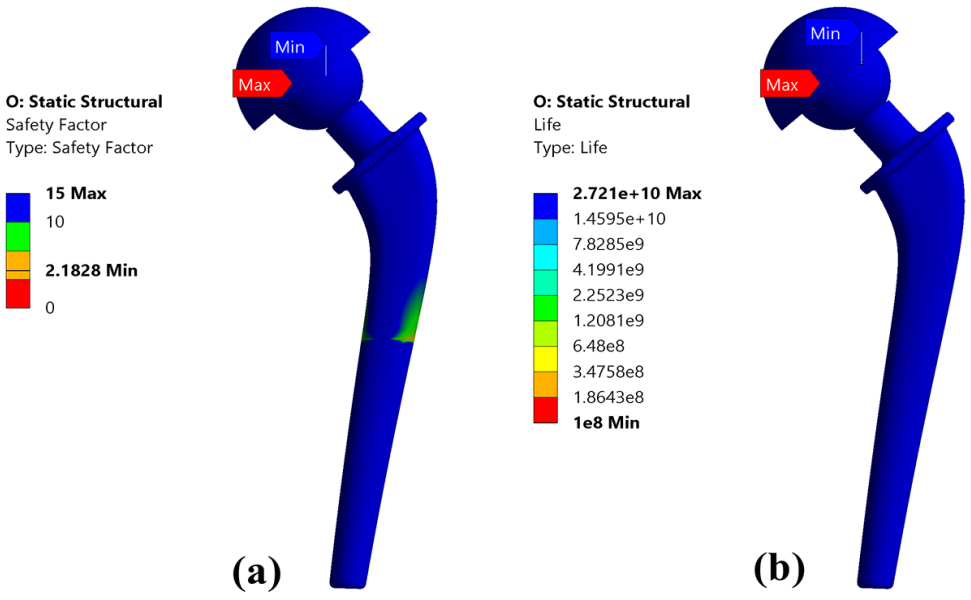

Figure 10: a) Factor of safety results across various radial clearances, **b**) Fatigue life outcomes for different material combinations

MC1 starts with a low FoS of approximately 1.5 at zero radial clearance, peaks at approximately 0.2 mm with an FoS slightly above 3.0 and declines sharply beyond this point. MC2 begins with an FoS of approximately 2.0 at zero clearance, gradually increases to a peak of approximately 3.2 at 0.25 mm, and then shows a slight decline. MC3 and MC4 exhibited the highest overall performance. It starts with a higher initial FoS of approximately 3.0 at zero clearance, peaks at 0.15–0.2 mm with a maximum FoS of approximately 4.5, and then experiences a minor decline.

Wear analysis

Wear analysis is crucial for hip implant longevity and affects the performance and patient outcomes [53]. The linear and volumetric wear rates depend on the radial clearance, which influences the load distribution and causes excessive material loss. Smaller clearances increase the contact stress, whereas larger clearances affect the kinematics, affecting wear patterns.

1. Linear wear rate for various radial clearances

Equation (3) was used to determine linear wear. To increase the lifespan of an implant, the wear rate must be decreased as much as feasible. One million cycles over a year were used to calculate the wear. The linear wear rate (in mm/year) for multiple material combinations across the HS, HL, and LA as a function of radial clearance of 0 mm to 0.3 mm is highlighted in Figure 12, which also displays the variation of linear wear rate (mm/year) for varying radial clearance for different material combinations under dynamic loading conditions.

The HS junction experiences the highest wear rates, particularly at smaller radial clearances, with MC1 peaking around 0.06 mm/year but showing a significant reduction as clearance increases. In contrast, MC3 and MC4 demonstrated excellent wear resistance, maintaining values below 0.02 mm/year throughout. The HL interface consistently exhibited lower wear rates than HS, with MC3 and MC4 standing out for their minimal wear below 0.02 mm/year. Meanwhile, the LA interface performs exceptionally well, with negligible wear rates below 0.01 mm/year for all material combinations and radial clearances.

2. Volumetric wear rate for various radial clearances

Equation (4) illustrates how to obtain the

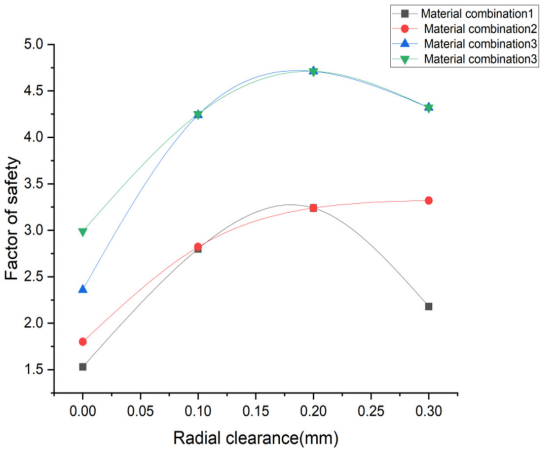

Figure 11: Relationship between radial clearance and factor of safety for various material combinations

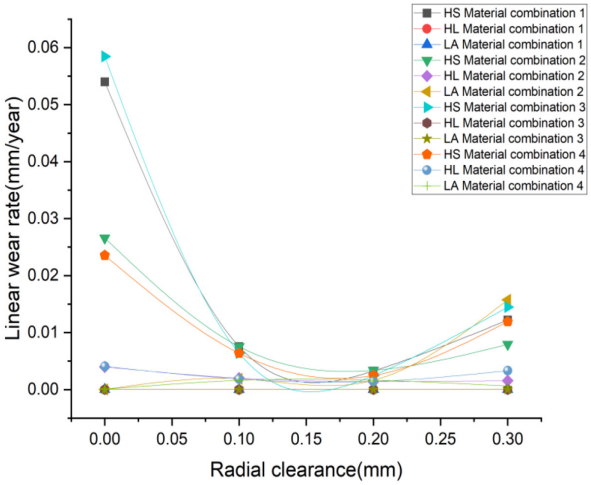

Figure 12: Comparative analysis of linear wear rates for different material combinations

volumetric wear rate by multiplying the linear wear rate by the contact area. Figure 13 shows the volumetric wear rates (in mm³/year) at interfaces HS, HL, and LA, as the radial clearance varies from 0 mm to 0.3 mm, and the variation in the volumetric wear rate (mm³/year) with different radial clearances.

The HS junction displays the highest wear rates, peaking at nearly 60 mm³/year for MC1 at minimal clearances, but wear significantly drops around 0.1 mm clearance before rising again. MC3 and MC4 emerged as top performers, maintaining wear rates below 20 mm³/year, even at smaller clearances. The HL interface exhibited moderate wear, with MC3 and MC4 standing out for their consistently low rates, staying under 10 mm³/year across all clearances. Meanwhile, the LA interface shines with negligible wear rates close to zero, showing remarkable stability and minimal dependence on the material combination or radial clearance.

Discussion

The findings from this study underscore the critical relationship between implant design parameters, material selection, and performance of hip prostheses during dynamic activities such as jogging [54]. The meticulous analysis of the newly designed hip implant's mechanical behaviour under various radial clearances and material combinations yields significant insights for optimizing both implant longevity and functionality.

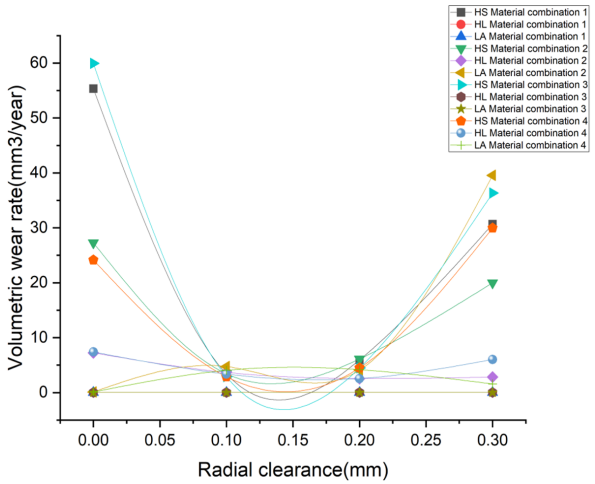

Figure 13: Comparative analysis of volumetric wear rates for different material combinations under dynamic loading conditions

Impact of Radial Clearance on Performance

Our results indicated a pronounced influence of radial clearance on the mechanical performance of hip implants. An optimal clearance of 0.2 mm was identified, providing a balanced distribution of contact pressure and reduced wear. Specifically, deformation analysis revealed a maximum total deformation of 0.0238 mm at a radial clearance of 0.3 mm, while von Mises stress peaked at 114.11 MPa at 0 mm clearance [55]. These results confirm that tighter clearances lead to increased contact stresses, potentially compromising the integrity of the implant over time. Thus, this study supports the principle that a well-optimized radial clearance enhances not only the performance but also the lifespan of the prosthesis under repetitive dynamic loads. The identification of a 0.2 mm clearance and durable material combinations offer practical guidance for implant selection, particularly for active patients requiring improved wear and fatigue resistance. Surgeons can apply these insights to refine implant alignment and procedural planning, while approaches for sedentary patients may focus on stability and long-term reliability to minimize failure risk.

Material Performance Insights

This study further elucidates the superiority of the Ti-6Al-4V alloy in terms of fatigue life and safety factors, particularly in high-impact scenarios. Fatigue analysis yielded an impressive FoS of approximately 4.5 at radial clearances between 0.15 mm and 0.2 mm for the optimal MC4. This performance, outperforming the FoS of 2.832 for the CoCr alloy alone, suggests that Ti-6Al-4V's robust

mechanical properties are particularly suited for high-stress applications such as jogging [40]. The fatigue life of the CoCr alloy reached approximately 3.8×10^{10} cycles, emphasizing its durability; however, the combination with Ti-6Al-4V alloy provides a more favourable safety margin, which is critical in mitigating failure risks during physical activities [56].

Wear Analysis and Recommendations

The wear analysis, conducted using Archard's model, highlighted the superior performance of MC3 (CoCr, UHMWPE, and Ti-6Al-4V). This combination recorded the lowest wear rates across all interfaces, most notably at the femoral head-stem junction, where wear is often most significant. This demonstrates that strategic material combinations specifically CoCr and UHMWPE paired with Ti-6Al-4V are effective in significantly reducing volumetric wear rates. Compared to the recorded linear wear rates of 0.07 to 0.6 mm/year, for existing metal or ceramic implants, these results represent a concrete advancement in hip implant design aimed at extended longevity [31,32].

The wear analysis performed using Archard's model showed that MC3, CoCr for the acetabular cup and femoral head, UHMWPE for the liner, and Ti-6Al-4V for the stem, exhibited the lowest wear rates, particularly at the femoral head–stem junction, where wear is typically most pronounced. These findings indicate that material combinations involving CoCr and UHMWPE, especially when paired with Ti-6Al-4V, significantly reduce volumetric wear rates. This suggests superior durability and suitability for active patients. Compared with reported linear wear rates of 0.07–0.6 mm/year, these results represent a meaningful improvement in implant design to minimize wear.

Dynamic Analysis

When analysing the sliding distances between components, our results indicate significant variation based on material combinations and radial clearances. Lower sliding distances across all junctions are desirable, as they correlate with reduced wear, micromotion, and improved implant stability. Higher sliding distances, particularly at the HS junction (fretting wear) and HL junction (bearing wear), highlight areas, where design optimization or coating improvements may be needed [57]. While specific combinations are optimal for certain junctions, enhanced mechanical performance ultimately hinges on a nuanced allocation of materials.

Excluding joint torque data may lead to underestimating localized stresses and wear, as impact forces from real gait dynamics, especially during high-impact activities like jogging, are not fully captured. Future studies should incorporate in vivo measurements of joint torques and experimental wear testing to validate finite element predictions, ensuring more accurate stress assessments and long-term wear behaviour, thereby enhancing the clinical relevance and reliability of the implant designs.

In conclusion, this study reinforces that meticulous consideration of both the radial clearance and material composition is paramount in the design of hip implants for active patients. These findings advocate the use of the CoCr-UHMWPE-Ti-6Al-4V alloy combination, particularly with an optimal radial clearance of 0.2 mm, to achieve superior wear resistance and fatigue life.

Although this study provides valuable insights into the mechanical performance of a newly designed hip implant, several limitations warrant a comprehensive analysis. First, the reliance on numerical simulations to evaluate mechanical performance metrics introduces uncertainties because these models may not fully capture the complexities of in vivo conditions. Real-world factors, such as biological interactions, load variances due to varied patient activity levels, and the multifactorial nature of human movement could

significantly influence the implant's performance over time, thereby affecting its clinical success [55].

Second, this research primarily focuses on idealized conditions when testing different material combinations and configurations. This approach may overlook critical patient-specific variables, such as bone quality, pre-existing medical conditions, and individual biomechanical differences, which are known to affect implant longevity and functioning. Consequently, the findings may not be universally applicable across diverse patient demographics, which limits the generalizability of the results.

Third, this study did not explicitly incorporate joint moment and torque data during jogging into the finite element models due to model complexity and data limitations. Instead, rotational and shear effects were approximated via boundary conditions reflecting gait dynamics, with the primary focus on contact stresses, material performance, and wear under axial loads.

The absence of long-term wear testing and evaluation of biological responses to wear particles represents a critical research gap. Archard's model, while widely applied, may not fully capture dynamic rotational and axial loads experienced during activities such as jogging, potentially leading to incomplete wear predictions. Incorporating lubrication modelling, such as elasto-hydrodynamic analysis, enables accurate simulation of fluid-film behaviour under dynamic loading [58]. Furthermore, experimental validation using pin-on-disk tests provides essential empirical data on friction, wear rates, and material performance, collectively enhancing prediction reliability and supporting optimized implant designs with improved durability [48].

Lastly, while this study emphasizes the importance of radial clearance in implant design, it does not investigate other critical design aspects such as optimal implant orientation or the efficacy of different surgical techniques. The omission of these factors may lead to incomplete conclusions regarding the overall effectiveness of the proposed implant design.

The limitations of this study suggest that, although the findings contribute to our understanding of hip prostheses, comprehensive future research is warranted. This research should integrate real-life clinical scenarios, patient-specific variables, and longitudinal data to fully validate the proposed designs. Addressing these limitations is paramount for establishing the clinical applicability and improving the long-term success rate of hip implants in active patient populations.

Conclusion

This study significantly advances the understanding of hip prosthesis performance under dynamic loading conditions, particularly during high-impact activities, such as jogging. By evaluating various radial clearances and material combinations, this research identifies an optimal radial clearance of 0.2 mm, which enhances wear resistance and fatigue life. These findings demonstrate that the CoCr-UHMWPE- Ti-6Al-4V alloy combination offers superior mechanical stability and durability, highlighting its potential for active patients who engage in high-impact sports.

The contributions of this study underscore the critical interplay between implant design, material selection, and operational performance, thereby providing a foundation for optimizing hip arthroplasty outcomes. However, the limitations related to the use of numerical simulations and the lack of long-term wear testing necessitate further research.

Future research should focus on conducting extensive in vivo studies to validate the numerical findings and explore the effects of patient-specific factors such as bone quality and activity levels on implant performance. Further research will need to investigate the long-term biological response to the proposed designs and assess the impact of varying surgical techniques and implant orientations.

These steps are essential to further refine hip prosthesis design strategies and enhance their clinical applicability.

Acknowledgment

The authors express their gratitude to the Department of Mechanical Engineering, PSG College of Technology, Coimbatore, India, for granting access to the high-performance computational facility essential for this research.

Authors' Contribution

K. M and D. P conceived the idea, created the graphs and figures, and drafted the manuscript. J. Reginald developed the theory, prepared the tables. Ch. K N. and N. Nikam verified the analytical methods and supervised the study's findings. All authors discussed the overall manuscript, contributed to the final manuscript and agreed to be accountable for all aspects of the work. All authors have read and agreed to the published version of the manuscript.

Ethical Approval

Ethical approval is not required for this research work.

Funding

This work is not received any funding.

Conflict of Interest

None

References

1. Alpkaya AT, Mihcin S. Sensitivity Analysis of Wear on Metal-On-Metal Bearing Couples via Verification of Numeric and Analytic Methods. *Hittite J Sci Eng.* 2024;**11**(2):57-67. doi: 10.17350/hjse19030000332.
2. Von Pückler KH, Tellhelm B, Kirberger RM. The hip joint and pelvis. In BSAVA manual of canine and feline musculoskeletal imaging. BSAVA; 2016. p. 212-32.
3. Rybski MF. The Hip and Pelvis. In Kinesiology for Occupational Therapy. 3rd Edition. Routledge; 2024. p. 291-303.
4. Mihcin S, Sahin AM, Yilmaz M, Alpkaya AT, Tuna M, Akdeniz S, et al. Database covering the prayer movements which were not available previously. *Sci Data.* 2023;**10**(1):276. doi: 10.1038/s41597-023-02196-x. PubMed PMID: 37173298. PubMed PMCID: PMC10182010.
5. Alpkaya AT, Yılmaz M, Şahin AM, Mihçin DŞ. Investigation of stair ascending and descending activities on the lifespan of hip implants. *Med Eng Phys.* 2024;**126**:104142. doi: 10.1016/j.medengphy.2024.104142. PubMed PMID: 38621844.
6. Solórzano W, Ojeda C, Diaz Lantada A. Biomechanical study of proximal femur for designing stems for total hip replacement. *Appl Sci.* 2020;**10**(12):4208. doi: 10.3390/APP10124208.
7. Balagna C, Faga MG, Spriano S. Tantalum-based multilayer coating on cobalt alloys in total hip and knee replacement. *Mater Sci Eng C.* 2012;**32**(4):887-95. doi: 10.1016/j.msec.2012.02.007.
8. Lu TW, Chang CF. Biomechanics of human movement and its clinical applications. *Kaohsiung J Med Sci.* 2012;**28**(2 Suppl):S13-25. doi: 10.1016/j.kjms.2011.08.004. PubMed PMID: 22301008. PubMed PMCID: PMC11922132.
9. Kuster MS. Exercise recommendations after total joint replacement: a review of the current literature and proposal of scientifically based guidelines. *Sports Med.* 2002;**32**(7):433-45. doi: 10.2165/00007256-200232070-00003. PubMed PMID: 12015805.
10. Kalayarasan M, Prakash L, Shankar S. Material selection of acetabular component in human hip prosthesis using finite element concepts. *Int J Exp Comput Biomech.* 2013;**2**(2):118-35. doi: 10.1504/ijecb.2013.056519.
11. Alpkaya AT, Mihçin Ş. The computational approach to predicting wear: comparison of wear performance of CFR-PEEK and XLPE liners in total hip replacement. *Tribol Trans.* 2023;**66**(1):59-72. doi: 10.1080/10402004.2022.2140727.
12. Holzer LA. Total Hip Arthroplasty: So Hip It Hurts. *J Clin Med.* 2023;**12**(11):3849. doi: 10.3390/jcm12113849. PubMed PMID: 37298044. PubMed PMCID: PMC10253778.
13. Evans JT, Evans JP, Walker RW, Blom AW, Whitehouse MR, Sayers A. How long does a hip replacement last? A systematic review and meta-analysis of case series and national registry reports with more than 15 years of follow-up. *Lancet.* 2019;**393**(10172):647-54. doi: 10.1016/S0140-6736(18)31665-9. PubMed PMID: 30782340. PubMed PMCID: PMC6376618.
14. Lee A, Paiement GD, Penenberg BL, Rajaee SS. Metallosis in Total Hip Arthroplasty. *JBJS Rev.* 2023;**11**(10):e23.00105. doi: 10.2106/JBJS.RVW.23.00105. PubMed PMID: 37812668.
15. Panwar K, Cutter B, Holmboe M, Card R, Pistel W, Law JI. Instability in total hip arthroplasty. In Arthroplasty-Advanced Techniques and Future Perspectives. IntechOpen; 2023.

16. Khalifa AA, Bakr HM. Updates in biomaterials of bearing surfaces in total hip arthroplasty. *Arthroplasty.* 2021;**3**(1):32. doi: 10.1186/s42836-021-00092-6.
17. Goriainov V, Cook R, M Latham J, G Dunlop D, Oreffo RO. Bone and metal: an orthopaedic perspective on osseointegration of metals. *Acta Biomater.* 2014;**10**(10):4043-57. doi: 10.1016/j.actbio.2014.06.004. PubMed PMID: 24932769.
18. Sathishkumar S, Paulraj J, Chakraborti P, Muthuraj M. Comprehensive Review on Biomaterials and Their Inherent Behaviors for Hip Repair Applications. *ACS Appl Bio Mater.* 2023;**6**(11):4439-64. doi: 10.1021/acsabm.3c00327. PubMed PMID: 37871169.
19. Whitehouse M, Patel R, French J, Beswick A, Navvuga P, Marques E, et al. Bearing Surface Materials and the Risk of Revision Following Primary Total Hip Arthroplasty: a Cohort Analysis of 1,026,481 Hip Arthroplasties From the National Joint Registry. In Orthopaedic Proceedings. *Orthop Procs.* 2024;**106**(SUPP_6):17-17. doi: 10.1302/1358-992X.2024.6.017.
20. Thöne P, Gruber MS, Kindermann H, Gussner W, Sadoghi P, Ortmaier R. Stem Design in Total Hip Arthroplasty Influences Ipsilateral Knee Valgus: A Retrospective Comparative Analysis of 2953 Cases. *J Clin Med.* 2023;**12**(20):6662. doi: 10.3390/jcm12206662. PubMed PMID: 37892800. PubMed PMCID: PMC10607773.
21. Burchard R, Graw JA, Soost C, Schmitt J. Stress shielding effect after total hip arthroplasty varies between combinations of stem design and stiffness-a comparing biomechanical finite element analysis. *Int Orthop.* 2023;**47**(8):1981-7. doi: 10.1007/s00264-023-05825-7 PubMed PMID: 37269400. PubMed PMCID: PMC10345085.
22. Hung JP, WU JS. A comparative study on wear behavior of hip prosthesis by finite element simulation. *Biomed Eng Appl Basis Commun.* 2002;**14**(04):139-48. doi: 10.4015/S1016237202000218.
23. Castagnini F, Bordini B, Cosentino M, Tassinari E, Guizzardi G, Traina F. Comparison of single taper and dual taper versions of the same stem design in total hip arthroplasty for primary osteoarthritis. *J Orthop Traumatol.* 2023;**24**(1):5. doi: 10.1186/s10195-023-00687-6. PubMed PMID: 36725766. PubMed PMCID: PMC9892395.
24. Jansson M, Similä H, Harjumaa M, Koivisto J, Haljas K, Lind M, et al. Co-design of a digital solution for total hip and knee arthroplasty journey: A case study. *FinJeHeW.* 2023;**15**(4):470-83. doi: 10.23996/fjhw.131314.
25. Learmonth ID, Young C, Rorabeck C. The operation of the century: total hip replacement. *Lancet.* 2007;**370**(9597):1508-19. doi: 10.1016/S0140-6736(07)60457-7. PubMed PMID: 17964352.
26. Pathak PK, Gupta RK, Meena HS, Fiske R. Limb length discrepancy after total hip arthroplasty: a systematic review. *Int J Res Orthop.* 2018;**4**(5):690. doi: 10.18203/issn.2455-4510.intjresorthop20183670.
27. Mueller S, Ahmad I, Kraemer M, Utz M, Gaa J, Kahrs LA, Ortmaier T. Design considerations for patient-specific surgical templates for total hip arthroplasty with respect to acetabular cartilage. *Biomed Tech (Berl).* 2017;**62**(3):263-9. doi: 10.1515/bmt-2016-0020. PubMed PMID: 27371818.
28. Rutsky AV. Total hip arthroplasty with own design endoprosthesis. *NN Priorov J Traumatol Orthop.* 2000;**7**(4):34-8. doi: 10.17816/vto104421.
29. Shaikh N, Shenoy B S, Bhat N S, Shetty S, KN C. Wear estimation at the contact surfaces of oval shaped hip implants using finite element analysis. *Cogent Eng.* 2023;**10**(1):2222985. doi: 10.1080/23311916.2023.2222985.
30. Benabid Y, Chettibi T, Benfriha K, Aoussat A. Design of innovative total hip prosthesis: Custom concepts. 4th IEEE RAS & EMBS International Conference on Biomedical Robotics and Biomechatronics (BioRob); Rome, Italy: IEEE; 2012. p. 878-83.
31. Kamecka K, Rybarczyk-Szwajkowska A, Staszewska A, Engelseth P, Kozlowski R. Process of Posthospital Care Involving Telemedicine Solutions for Patients after Total Hip Arthroplasty. *Int J Environ Res Public Health.* 2021;**18**(19):10135. doi: 10.3390/ijerph181910135. PubMed PMID: 34639436. PubMed PMCID: PMC8508342.
32. Niu F, Zhang K, Han J, Xu M, Wang J, Jiang N, et al. Fabrication of TC4/TiCp New Hip Prosthesis by Laser Cladding. *Adv Eng Mater.* 2023;**25**(19):2300517. doi: 10.1002/adem.202300517.
33. Rafiq NM, Wang W, Liew SL, Chua CS, Wang S. A review on multifunctional bioceramic coatings in hip implants for osteointegration enhancement. *Appl Surf Sci Adv.* 2023;**13**:100353. doi: 10.1016/j.apsadv.2022.100353.
34. Khalifa AA, Bakr HM, Farouk OA. Biomaterials and technologies in the management of periprosthetic infection after total hip arthroplasty: an updated review. *J Musculoskelet Surg Res.* 2021;**5**(3):142-51. doi: 10.25259/JMSR_51_2021.
35. Hailer NP, Weiss RJ, Stark A, Kärrholm J. The risk of revision due to dislocation after total hip arthroplasty depends on surgical approach, femoral head size, sex, and primary diagnosis. An analysis of 78,098 operations in the Swedish Hip Arthroplasty Register. *Acta Orthop.* 2012;**83**(5):442-8. doi: 10.3109/17453674.2012.733919. PubMed PMID: 23039167. PubMed PMCID: PMC3488169.
36. Baumann J, Marshall S, O'Malley J, DeFroda S. A standardised method for improving the readability of patient education materials for total hip & knee arthroplasty patients. *Musculoskeletal Care.*

2024;**22**(1):e1862. doi: 10.1002/msc.1862.

37. Chang JD. Future bearing surfaces in total hip arthroplasty. *Clin Orthop Surg.* 2014;**6**(1):110-6. doi: 10.4055/cios.2014.6.1.110. PubMed PMID: 24605198. PubMed PMCID: PMC3942597.
38. Fontalis A, Epinette JA, Thaler M, Zagra L, Khanduja V, Haddad FS. Advances and innovations in total hip arthroplasty. *SICOT J.* 2021;**7**:26. doi: 10.1051/sicotj/2021025. PubMed PMID: 33843582. PubMed PMCID: PMC8040589.
39. Varnum C, Pedersen AB, Rolfson O, Rogmark C, Furnes O, Hallan G, et al. Impact of hip arthroplasty registers on orthopaedic practice and perspectives for the future. *EFORT Open Rev.* 2019;**4**(6):368-76. doi: 10.1302/2058-5241.4.180091. PubMed PMID: 31210974. PubMed PMCID: PMC6549115.
40. Reginald J, M K, KN C, P D. Static, dynamic, and fatigue life investigation of a hip prosthesis for walking gait using finite element analysis. *Int J Model Simul.* 2023;**43**(5):797-811. doi: 10.1080/02286203.2023.2212346.
41. K NC, Zuber M, Bhat NS, Shenoy BS. Optimized trapezoidal-shaped hip implant for total hip arthroplasty using finite element analysis. *Cogent Eng.* 2020;**7**(1):1719575. doi: 10.1080/23311916.2020.1719575.
42. Tauviqirrahman M, Ammarullah MI, Jamari J, Saputra E, Winarni TI, Kurniawan FD, et al. Analysis of contact pressure in a 3D model of dual-mobility hip joint prosthesis under a gait cycle. *Sci Rep.* 2023;**13**(1):3564. doi: 10.1038/s41598-023-30725-6. PubMed PMID: 36864170. PubMed PMCID: PMC9981612.
43. Gutmann C, Shaikh N, Shenoy BS, Shaymasunder Bhat N, Keni LG, KN C. Wear estimation of hip implants with varying chamfer geometry at the trunnion junction: a finite element analysis. *Biomed Phys Eng Express.* 2023;**9**(3):035004. doi: 10.1088/2057-1976/acb710. PubMed PMID: 36716460.
44. Tirosh O. 3D Gait Analysis to Identify Running Injury Risk. In: Melb Sport Allied Heal Clin. 2016. Available from: https://msahc.com.au/news/3d-gait-analysis-to-identify-running-injury-risk.
45. Bergmann G, Bender A, Dymke J, Duda G, Damm P. Standardized Loads Acting in Hip Implants. *PLoS One.* 2016;**11**(5):e0155612. doi: 10.1371/journal.pone.0155612. PubMed PMID: 27195789. PubMed PMCID: PMC4873223.
46. Mihçin Ş, Ciklacandir S. Towards integration of the finite element modeling technique into biomedical engineering education. *Biomed Eng Appl Basis Commun.* 2022;**34**(02):2150054. doi: 10.4015/S101623722150054X.
47. ASTM. F. 2996-20 Standard Practice for Finite Element Analysis (FEA) of Non-Modular Metallic Orthopaedic Hip Femoral Stems. ASTM; 2020.
48. Basri H, Syahrom A, Prakoso AT, Wicaksono D, Amarullah MI, Ramadhoni TS, Nugraha RD. The analysis of dimple geometry on artificial hip joint to the performance of lubrication. *J Phys Conf Ser.* 2019;**1198**(4):042012. doi: 10.1088/1742-6596/1198/4/042012.
49. Bergmann G, Deuretzbacher G, Heller M, Graichen F, Rohlmann A, Strauss J, Duda GN. Hip contact forces and gait patterns from routine activities. *J Biomech.* 2001;**34**(7):859-71. doi: 10.1016/s0021-9290(01)00040-9. PubMed PMID: 11410170.
50. Atar E. Sliding wear performances of 316 L, Ti6Al4V, and CoCrMo alloys. *Kovove Mater.* 2013;**51**(3):183-8.
51. Anticona Valderrama DM, Serna-Landivar JL, Algoner WC, Miranda ML, Garcia-Alvarez MY, Serna Landivar LK. Static, Transient, and Fatigue Design and Analysis of a Hip Femoral Stem Using the Finite Element Method. *Int J Online Biomed Eng.* 2024;**20**(16):89-102. doi: 10.3991/ijoe.v20i16.52865.
52. Darwich A, Nazha H, Daoud M. Effect of coating materials on the fatigue behavior of hip implants: A three-dimensional finite element analysis. *J Appl Comput Mech.* 2020;**6**(2):284-95. doi: 10.22055/jacm.2019.30017.1659.
53. Alpkaya AT, Mihcin S. Dynamic computational wear model of PEEK-on-XLPE bearing couple in total hip replacements. *Med Eng Phys.* 2023;**117**:104006. doi: 10.1016/j.medengphy.2023.104006. PubMed PMID: 37308373.
54. Abe H, Sakai T, Nishii T, Takao M, Nakamura N, Sugano N. Jogging after total hip arthroplasty. *Am J Sports Med.* 2014;**42**(1):131-7. doi: 10.1177/0363546513506866. PubMed PMID: 24114754.
55. Torabnia S, Mihcin S, Lazoglu I. Design and manufacturing of a hip joint motion simulator with a novel modular design approach. *Int J Interact Des Manuf.* 2024;**18**(1):401-17. doi: 10.1007/s12008-023-01506-2.
56. Corda JV, Chethan KN, Shenoy S, Shetty S, Zuber M. Fatigue life evaluation of different hip implant designs using finite element analysis. *J Appl Eng Sci.* 2023;**21**(3):896-907. doi: 10.5937/jaes0-44094.
57. K NC, Ogulcan G, Bhat NS, Zuber M, Shenoy BS. Wear estimation of trapezoidal and circular shaped hip implants along with varying taper trunnion radiuses using finite element method. *Comput Methods Programs Biomed.* 2020;**196**:105597. doi: 10.1016/j.cmpb.2020.105597. PubMed PMID: 32574903.
58. Ruggiero A, Sicilia A. A mixed elasto-hydrodynamic lubrication model for wear calculation in artificial hip joints. *Lubricants.* 2020;**8**(7):72. doi: 10.3390/LUBRICANTS8070072.